Proceedings World Geothermal Congress 2026
Calgary, Canada, June 8 – 11, 2026

Unlocking the Potential of Flooded Mines: Economic Analysis of integrating Carnot Batteries for Heating and Electricity

A. Cendoya[1]*, F. Ransy[1], B. Guo[1], P.H. Gresse[2], A. Hernandez[1] and V. Lemort[1]
Thermodynamics Laboratory, Faculty of Applied Sciences,
University of Liège, Liège, Belgium[1]
Flexide Energy, Liège, Belgium[2]
*Corresponding author: acendoya@uliege.be

Keywords: Seasonal Storage, Renewable Energy Integration, Massive Energy Storage, Heat Pump, Organic Rankine Cycle

ABSTRACT

Many countries are progressing towards energy systems largely based on renewable resources. To enable this transition, it is essential to develop new solutions for reliable and flexible energy storage and distribution. Flooded abandoned mines offer high potential to host local energy communities, more than 9000 such sites exist in Europe alone, given the opportunity to act as large-scale thermal storage systems and providing services that support grid stability. Within the framework of the European WeForming project, this study investigates the economic analysis of a flooded mine in southern Belgium as a multi-service demonstrator for heating and electricity dispatch. The mine infrastructure enables daily, weekly and seasonal thermal storage using several flooded caverns: 6000 m^3 at 45–55 °C, 10000 m^3 at 25–40 °C, and 120000 m^3 at 15–25 °C. In addition, a 350000 m^3 volume at 8–10 °C serves as a cold sink. A yearly simulation model developed in Python is presented alongside the construction progress of the demonstrator, which is expected to be fully operational by mid-2026. On the demand side, the system is designed to provide services to the electricity grid, participate in the day-ahead market, supply process heat at 120 °C to an industrial consumer, and deliver low-temperature heat to a district heating network (DHN). The results demonstrate the strong techno-economic potential of the concept, with a Levelized Cost of Energy (LCOE) of 310.85 €/MWh for the whole system, decreasing significantly when only the CB subsystem is considered (209.21 €/MWh), and even further when grid taxes are excluded, reaching values around 108.72 €/MWh. The discounted payback period is about 23.8 years for the entire system but falls to 6.21 and 3.51 years for the CB, depending on the inclusion of taxes. These results are based on real performance and cost data, underlining the relevance of flooded mines as multi-service assets and motivating further research and deployment.

1 INTRODUCTION

The growing penetration of renewable energy sources into the electricity grid, together with the increasing demand for heat in several industrial sectors aiming to electrify and replace fossil fuels, has intensified the need for flexible and dispatchable multi-energy hubs. However, this is not exempt from problems; the variability of renewables and the progressive decommissioning of conventional fossil fuel power plants place additional stress on the grid. As a result, energy storage systems have become essential for frequency stability, balancing supply and demand, improving flexibility, and supporting a secure energy transition (Nitsch et al., 2024). Carnot Batteries (CBs) can be designed as large-scale electricity storage technologies and multi-energy hubs, capable of providing electricity, heating and/or cooling (Lykas et al., 2026), with advantages such as high energy density, long service life, and minimal geographical constraints (Frate et al., 2020). CBs convert surplus electricity into heat via a power-to-heat cycle and subsequently reconvert this heat into electricity via a heat-to-power cycle. Although CBs have been studied in several applications, their integration into flooded abandoned mines remains a novel research field. Given the large number of such sites worldwide, nearly 9000 in Europe alone, this concept offers significant deployment potential (Pinto et al., 2020). Despite their technical challenges, abandoned flooded mines offer a unique opportunity for large-scale thermal energy storage and for serving as multi-energy hubs. In this context, techno-economic assessments are critical to establishing the economic viability of such concepts. However, to date, no techno-economic studies of CB systems coupled with flooded mines have been reported. This work presents the first comprehensive economic assessment of integrating a reversible CB system into abandoned flooded mines in an industrial context, thereby demonstrating and quantifying its potential for real-world application. Operating with a heat pump (power-to-heat) and an Organic Rankine Cycle (heat-to-power), in an industrial case study. The analysis uses real market prices and operating conditions from

the demonstrator currently under construction within the European WeForming project, as described by (Ransy et al., 2026)

2 CASE STUDY

The case analysed is based on the demonstrator introduced by (Ransy et al., 2026). The present extrapolation increases the useful volumes of the real mine cavities (the installed capacity of the solar thermic panels, the overground thermal storage tank, and the electric resistance heater capacity) and introduces an industrial client. Whereas the reversible CB is kept at the same machine power (nominal 50kWe and 600 kWth). A schematic of the Rankine-based CB coupled to the flooded mine, depicting the charging and discharging pathways for heat, electricity, and cooling, is provided in Figure 1.

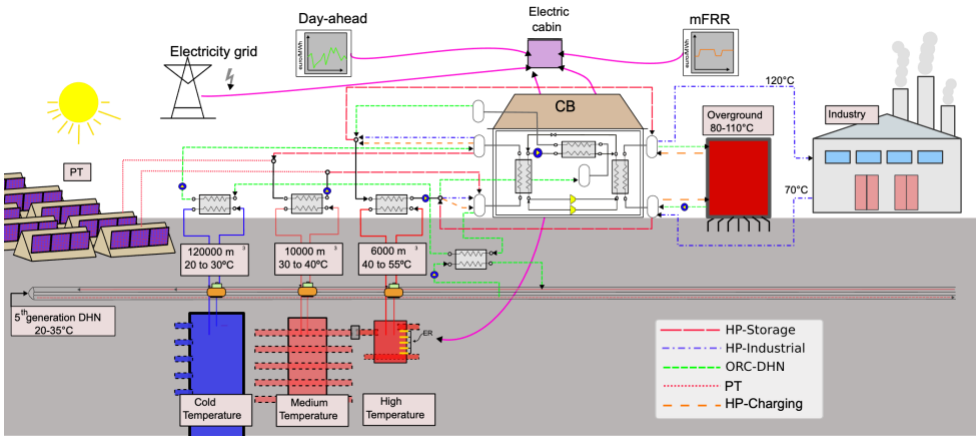

Figure 1. Case study of flooded mine coupled with Rankine CB for providing heating, electricity and cooling.

The site is an abandoned slate mine, located in Martelange, Belgium, formerly exploited via underground chamber-and-pillar methods, and decommissioned in the 1990s following a loss of economic viability. Nowadays is flooded with approximately 500000 m^3, distributed across nine cavities whose depth increases from east to west.

The integrated Rankine CB comprises multiple sources/sinks and operating modes that interact with underground storage: CT (Cold-temperature), MT (medium-temperature), HT (high-temperature) and the overground hot-water tank. The operational modes considered are:

- HP–Storage; The Rankine CB operates as a heat pump, extracting heat from the MT underground storage at the evaporator and upgrading it at the condenser to charge the HT underground storage.
- HP–Industrial; When the industrial client requests heat during specified hours, the industrial return water is sent to the HP condenser and upgraded to 120°C for process use.
- ORC–DHN; The Rankine CB operates as an ORC, generating electricity from heat drawn from the overground hot-water tank. The cycle's condenser rejects heat to the DHN return.
- PT: Thermal energy from the solar thermal collectors is stored in the MT underground storage.
- HP–Charging; When the overground hot-water tank temperature reaches its lower threshold (85°C), the HP extracts heat from the HT underground storage until it restores the tank to its maximum temperature (110°C).

Moreover, 2MW of electric resistance are integrated to charge the MT and HT underground storage during periods of surplus electricity or when the electricity prices are low. It is important to note the thermodynamic implications of the different operation modes. In general, during HP mode, the Rankine CB upgrades heat for delivery to high-temperature uses. In ORC mode, it converts stored heat to electricity, whereas the heat rejection is used in the DHN return.

3 MODELLING

The modelling involves the description of the main components, such as the reversible Heat Pump/Organic Rankine Cycle (CB), underground storage and overground tank.

3.1 CARNOT BATTERY

The reversible CB corresponds shares almost all the components in both operational cycles. HP mode delivers heat, whereas ORC mode produces electricity. The only difference lies in the volumetric machines, where a dedicated compressor and expander are chosen, instead of using one for both modes. The machine components and the P&ID have been very well detailed in a previous study (Cendoya et al., 2025). The numerical modelling in this study considers detailed part-load models of several components: heat exchangers, expander, compressor, piping, pumps and liquid receiver. A moving-boundary approach for the heat exchangers, semi-empirical models for the compressor and the expander, and nondimensional performance factors for the pumps. Moreover, heat-transfer, void-fraction, and pressure-drop correlations are integrated for the piping circuits and the heat exchangers. For further information on the modelling, please refer to the following references, where the machine has been extensively documented (Cendoya et al., 2024; Cendoya et al., 2026). Figure 2 presents a schematic of the CB model with global inputs, parameters, control laws, and outputs. All the parameters considered correspond to the real components employed in the machine, which has a nominal capacity of 600 kW_{th} and 50 kWe.

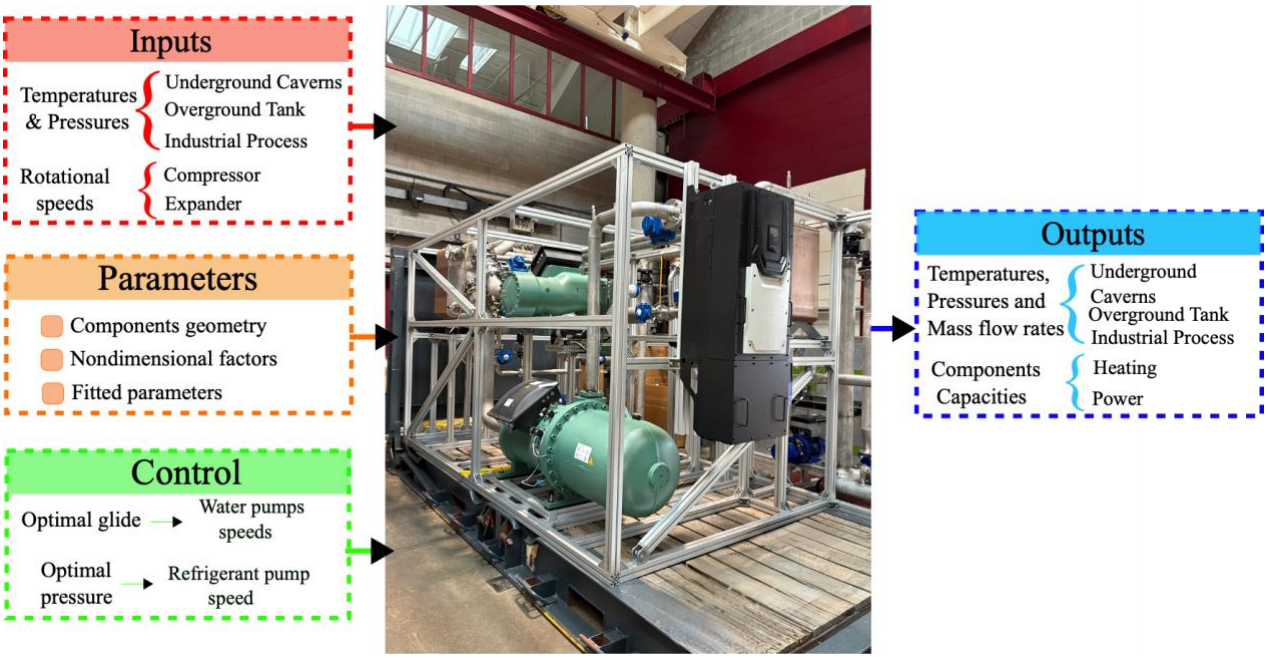

Figure 2. Reversible Heat Pump/Organic Rankine Cycle modelling summary.

The main performance indicators of the machine are presented in Figure 3, showing the Coefficient of Performance (COP) for the HP mode and the electrical efficiency (η_{ORC}) of the ORC. These two parameters are defined as follows: the COP is the ratio of the heat produced ($\dot{Q}_{cd,HP}$) to the total power required for operation, compressor and auxiliaries ($\dot{W}_{cp,HP} + \sum \dot{W}_{sf,pp}$). For the ORC efficiency, it is the ratio of net power produced (expander minus pump and auxiliaries) ($\dot{W}_{exp,ORC} - \dot{W}_{pp,ORC} - \sum \dot{W}_{sf,pp}$) against the heat supplied to the ORC evaporator ($\dot{Q}_{ev,ORC}$).

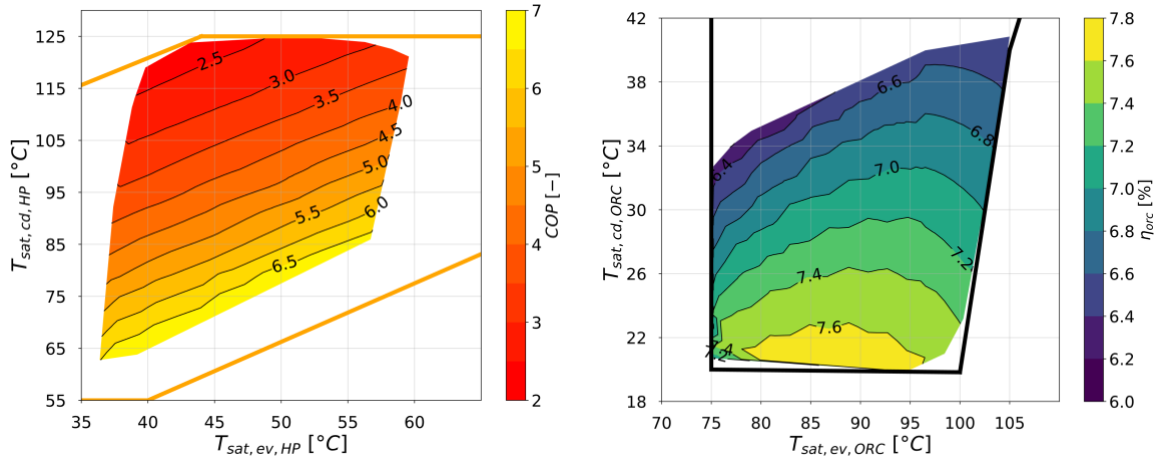

Figure 3. Map performance indicators for the HP (right) and ORC (left).

$$COP = \frac{\dot{Q}_{cd,HP}}{\dot{W}_{cp,HP} + \sum \dot{W}_{sf,pp}} \quad (1)$$

$$\eta_{ORC} = \frac{\dot{W}_{exp,ORC} - \sum \dot{W}_{sf,pp} - \dot{W}_{pp,ORC}}{\dot{Q}_{ev,ORC}} \quad (2)$$

3.2 Underground storages and overground tank

The underground cavities and the overground tank are modelled as a single, well-mixed reservoir. Thermal stratification is neglected, and it is assumed that the entire storage volume has a uniform temperature, which evolves over the simulation time. The energy balance for the medium-temperature storage is presented in equation 3. Here, $T_{MT}^{(i)}$ is the storage temperature at the time step i, $M_{w,MT}$ is the water mass in the storage, $c_{p,w,MT}$ is the specific heat capacity of water in the storage, and ΔU is the net thermal energy added or drawn from the storage during the time step, which is defined by equation 4. These equations are general for the different types of storage in the case study.

$$T_{MT}{}^{(i)} = T_{MT}{}^{(i-1)} + \frac{\Delta U}{M_{w,MT} \cdot c_{p,w,MT}} \quad (3)$$

$$\Delta U = \int_{t=i-1}^{t=i} \sum_{j=0}^{j=5} (\dot{Q}_{mode,j} - \dot{Q}_{loss,MT})\, dt \quad (4)$$

The thermal power of the different operating modes is transferred to the heat exchangers ($\dot{Q}_{mode,j}$), where this, minus the heat loss from the storage tanks ($\dot{Q}_{loss,MT}$), is responsible for varying the internal energy in the different tanks. Here, heat losses are considered constant throughout the simulation, and the value considered corresponds to 500 W/m^3, values taken from the reference (Cendoya et al., 2024), for underground caverns after 4 years of operation.

3.3 Thermal panels and electrical resistance

The power data for the thermal panels are obtained from (Ransy et al., 2026), where the model is explained and detailed. In this work, the same data sets and assumptions are adopted; the power is not extrapolated. Furthermore, it is assumed that the electrical resistors convert all electrical energy into heat.

4 ECONOMIC MODEL

The economic analysis is based on the components purchased as part of the demonstrator presented (Ransy et al., 2026). Prices for specific volumes and power ratings are extrapolated to the present case study. Furthermore, the cost of the CB for the machine evaluated to produce heat and electricity is introduced here for the first time. It should be noted that the prices considered here may overestimate the actual cost, with particular emphasis on underground storage, where expenses are mainly related to the connection of underground mines and not to the available volume.

Table 1 presents the Capital Expenditures (CAPEX) for the construction of the case study and the Operational Expenditures (OPEX). The cost data for the CB correspond to the same equipment that will be integrated into the demonstrator. In contrast, the underground storage, overground tank, and electrical resistance costs are extrapolated from the real demonstrator.

Table1. CAPEX of the installations considered in this assessment

Component	Capacity	C_{inv} (k€)	Unit price	Estimation
Underground sto.	16000 m^3 (total)	319	20 €/m^3	Extrapolated
CB machine	50 kWe-600 kWth	376.3	7526 €/kWe - 621 €/kWth	Demostrator

Overground tank	30 m^3	38	1266 €/m^3	Extrapolated
Electrical Resistances	2000 kW	198.0	99 €/kW	Extrapolated

For operating costs, in several cases 1.5%of the component CAPEX is applied, as stated in the cited reference. For the thermal panels (PT), the same operational cost as for photovoltaic panels is used, due to the similarity of balance-of-plant and maintenance needs. The system lifetime (LT) is 25 years and is limited by the thermal panels. A discount rate (r) value of 5% is used throughout the economic model.

Total investment cost aggregates all assets:

$$C_{inv} = C_{inv,CB} + C_{inv,sto} + C_{inv,tk} + C_{inv,PT} + C_{inv,ER} \tag{5}$$

As the submersible pump and the filtration system of the underground storage have shorter lifetimes than the rest of the plant, their replacements are included at 10-year (n) intervals in equation 6, where 78500 € and 64000 € are the pump and filtration replacement.

$$C_{inv,sto} = C_{inv,und,sto} + \sum_{i=1}^{LT/n} \frac{1}{(1+r)^n} \cdot (78500 + 64000) \tag{6}$$

The annual OPEX is the sum over components, where for each component the equations are obtained from Guo et al., (2025):

$$C_{OM} = C_{OM,CB} + C_{OM,sto} + C_{OM,tk} + C_{OM,PT} + C_{OM,ER} \tag{7}$$

The annual energy generated term combines net electricity from the ORC and equivalent electrical energy savings to useful heat via theoretical Carnot efficiencies. Here, $\dot{W}_{net,ORC}$ is the annual net electric output (MWh_e/y), and $\dot{Q}_{ind}, \dot{Q}_{DHN}$ are the annual useful heats for the industrial process and DHN, respectively. The Carnot efficiencies correspond to 1.5 (45 % of Carnot efficiency) and 5 (25% of Carnot efficiency) for $COP_{th,ind}$ and $COP_{th,DHN}$, respectively. These values reflect different source/sink temperatures: 120°C, the hot sink for the industrial process, and 30°C for the DHN, both with a cold source temperature ambient of 15°C. The temperature difference between Industrial mode and DHN mode corresponds to industrial demand and typical temperatures for fifth-generation DHN.

$$E_{gen} = \int \dot{W}_{net,ORC} dt + \int \frac{\dot{Q}_{ind}}{COP_{th,ind}} dt + \int \frac{\dot{Q}_{DHN}}{COP_{th,DHN}} dt \tag{8}$$

Then the Levelized cost of energy (LCOE) is calculated as follows, with a discount rate of 5%:

$$LCOE = \frac{C_{inv} + \sum_{i=1}^{LT} \frac{C_{OM} + C_{a,grd}}{(1+r)^i}}{\sum_{i=1}^{LT} \frac{E_{gen}}{(1+r)^i}} \tag{9}$$

Then the Discounted Payback Period (DPP) is calculated as follows:

$$DPP = -\frac{1}{r} \cdot Ln\left[1 - \frac{C_{inv} \cdot (\exp(r) - 1)}{R_{CB} - C_{a,grid}}\right] \tag{10}$$

R_{CB} denotes the annual revenues attributable to the CB from both, electricity in the manual frequency restoration reserve (mFRR) market and heat sales to either the DHN or to the industrial client. The following prices are assumed:

- mFRR upwards: $C_{a,\mathrm{up}} = 250$ €/$\mathrm{MW}_e\mathrm{h}$
- mFRR downwards: $C_{a,\mathrm{down}} = 100$ €/$\mathrm{MW}_e\mathrm{h}$
- Heat sold to DHN: $C_{a,\mathrm{DHN}} = 45$ €/$\mathrm{MW}_{th}h$

- Heat sold to industry: $C_{a,\mathrm{ind}} = 70\ €/\mathrm{MW}_{th}h$

$$R_{CB} = E_{CB,MFRR,up} \cdot C_{a,up} + E_{CB,MFRR,down} \cdot C_{a,down} + \int \dot{Q}_{ind}\, dt \cdot C_{a,ind} + \int \dot{Q}_{DHN}\, dt \cdot C_{a,DHN} \quad (11)$$

Here, $E_{CB,MFRR,up}$ and $E_{CB,MFRR,down}$ corresponds to the annual electrical energies generated/consumed under upwards and downwards activations, respectively. Whereas $\dot{Q}_{ind}$ and $\dot{Q}_{DHN}$ are the annual useful heats delivered to the industrial client and DHN

5 SIMULACION

The full case-study model is implemented in Python. Thermophysical properties are obtained from the CoolProp library (Bell et al., 2014), and the optimisation of the modified Powell method is used to find the solution of the iteration process in each iteration. Simulations use 2024 data: day-ahead electricity prices from ENTSO-E, (2025), mFRR bids from the Belgian transmission system operator Elia , (2025).The simulation time step is 15 minutes, consistent with the mFRR product granularity. The industrial heating load is enforced for 7 hours per day (07:00–14:00), every day of the year. Outside this window, operation is driven by the flexibility market and electricity prices. The supervisory logic first ensures the thermal demand is met within and then responds to mFRR signals and day-ahead prices. Optimisation of the operation is beyond the scope of this work; the control is intentionally simple to highlight the potential of flooded abandoned mines to provide cross-process flexibility. Figure 4 illustrates day-ahead prices and flexible activations for days 83–84 of 2024, together with the industrial heating demand. In the analysis, mFRR activations for the standard and flexible are treated equivalently, making no distinction between the two contracts.

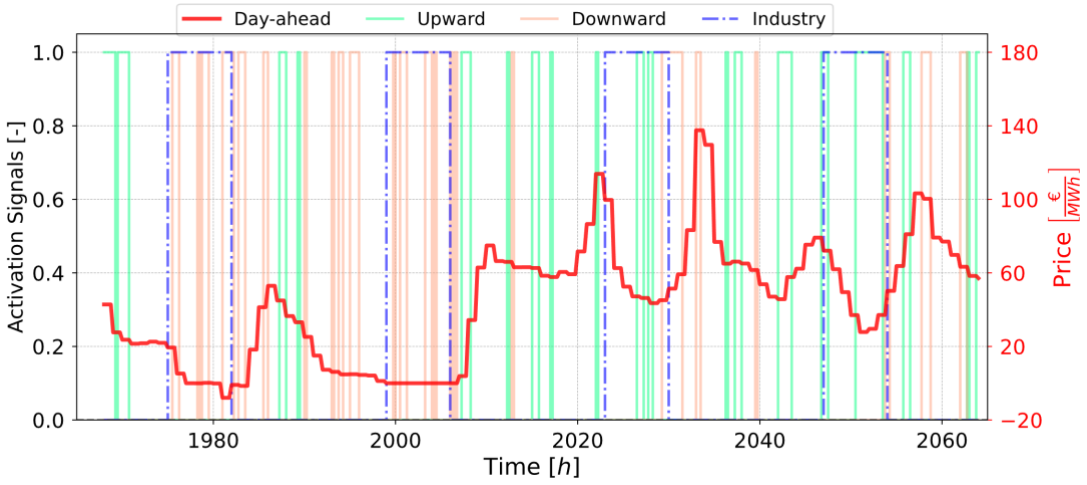

Figure 4. Day-ahead and mFRR activation for the 83-84 days of 2024.

The operational control strategy for the case study is illustrated in Figure 5, which summarises the decision-making sequence for the CB operation. The main thermal storage parameters considered are as follows: an above-ground tank of 30 m^3 with no heat losses; a low-temperature (LT) underground storage of 120000 m^3 with heat losses of 18 kW/h; a medium-temperature (MT) underground storage of 10000 m^3 with heat losses of 6 kW/h; and a high-temperature (HT) underground storage of 6000 m^3 with heat losses of 6 kW/h.

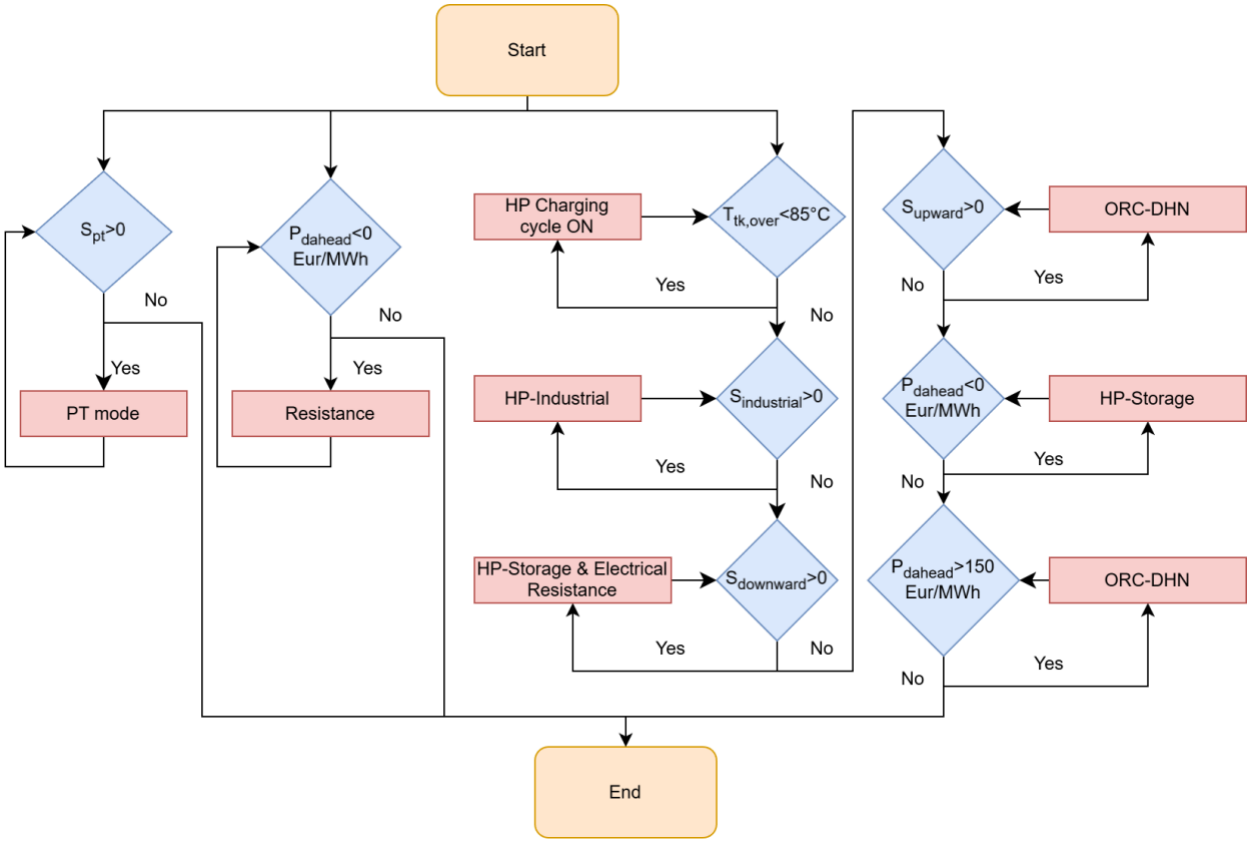

Figure 5. Control strategy for the system operation.

6 RESULTS

The results for the different energy flows and their contributions are presented in Figure 6, which shows the Sankey diagram representing all energy interactions within the whole system. This diagram illustrates the energy supplied by the electricity grid as well as the energy exchanged with the different storages and the major consumers and producers, the CB and the ERs. Moreover, it presents the various services that are covered within the CB (reversible HP/ORC).

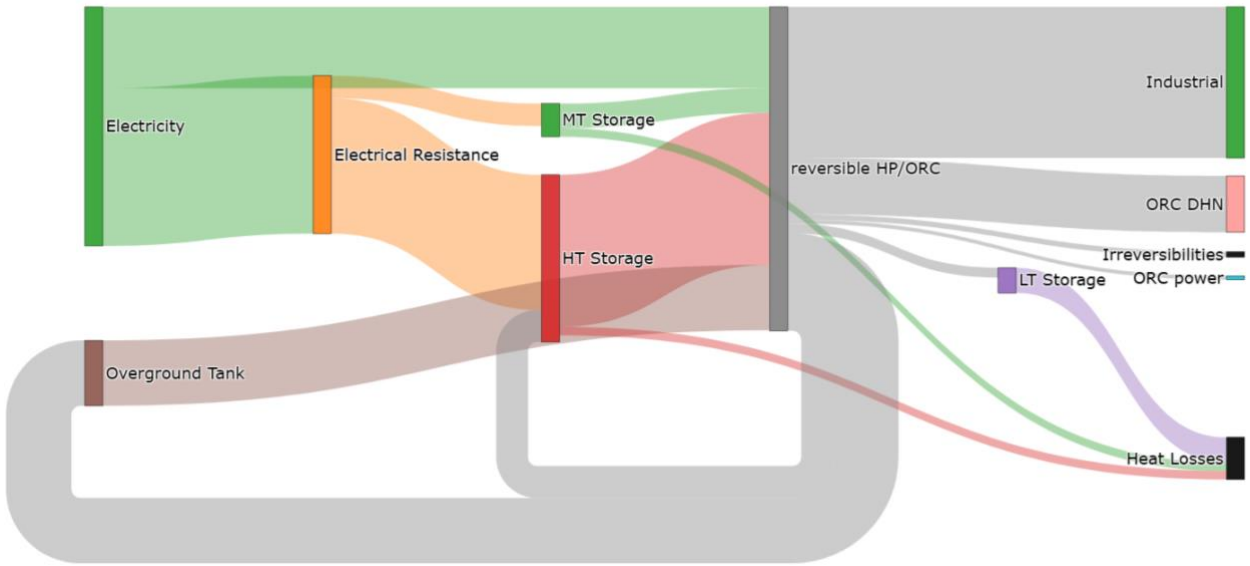

Figure 6. Sankey diagram for the simulation period (year 2024).

The largest share of incoming energy originates from the electricity grid (507 MWh to the CB and 984 to the ERs), the storage, which has a key role in the operation of the CB, supplying 949 and 153 MWh by the HT storage,

overground tank and MT storage. Highlighting the huge role of the HT feeding with heat, the CB operation and the relevance of the ER to produce this heat via the "waste electricity" (negative prices or downward signals). Becoming that this energy storage is crucial to adopt several control strategies or other methods to keep it warm, as it is the backbone of the CB operation, which can also be replaced by waste heat.

The CB subsequently dispatches 984 MWh of heat to an industrial client, which is the dominant output due to the implemented control strategy. Followed by the heat rejected to the DHN during ORC operation (351 MWh), the ORC power production (24 MWh) and the irreversibility, such as electromechanical inefficiencies and heat losses in the system. Overall, the CB handles approximately 2.02 GWh of energy throughout the year, where almost half is provided to industrial purposes, showing the high interest in industrial processes.

The largest portion of electrical input is directed to the ERs, which operate according to the control strategy and subsequently supply the CB. This ensures that the energy balance across the different storage units is maintained. Nevertheless, it is important to note that the underground storage units do not achieve a strict 1:1 energy balance at the end of the year. In reference to the initial conditions, the LT and MT storages show an energy deficit (ends with a lower temperature), while the HT storage ends with a surplus (ends with a higher temperature). This is normal as the operation of the machine was restricted to our operational strategy. Several different strategies can be applied and optimised to adjust the optimal balance and operation.

During the operation, all financial flows can be classified into three categories: revenues, costs, and fees. The third category refers to the taxes imposed by the Belgian Transmission and Distribution System Operators, which are applied as a fixed charge per MWh of electricity consumed. In this study, a value of 60 €/MWh was considered, and it is important to note that these fees are primarily associated with electricity purchased from the market. Frequency restoration actions are assumed to be exempt from these taxes.

Figure 7 presents these financial categories together with the operation modes that contribute to each of them. Here, the industrial client represents the largest source of revenue, and the main cost too from purchasing electricity from the grid whenever required. The highest grid fee is linked to the ER, rather than to industrial consumption or HP charging. This occurs because the ER operates intensively during periods of negative BELPEX prices. Even though negative prices yield a financial gain on the energy market, the system must still pay the fixed grid fee for every MWh consumed.

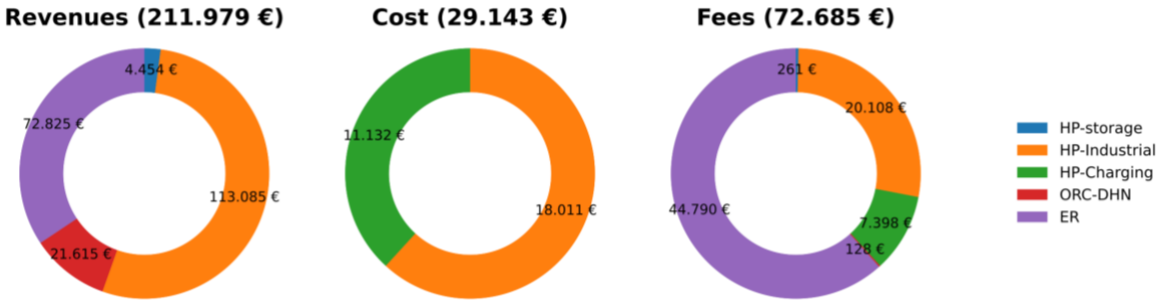

Figure 7. Revenues, Costs and Fees for the whole operation year

Using this information, the LCOE is evaluated under three scenarios. The first scenario considers the entire system, including the full installation. The second scenario includes only the CB together with the ERs, treated as a single integrated system. The third scenario considers only the CB, assuming that the heat previously supplied by the ERs is now provided by an external waste-heat source. For each scenario, two cases are analysed: with and without the fees from the TSO and DSO. Additionally, the analysis accounts for CO_2 related revenues associated with avoided emissions. The results clearly show the strong impact of grid fees on the LCOE, significantly increasing its value. For the complete installation, the LCOE reaches 310 €/MWh. When only the CB and ERs are considered, the LCOE decreases to 209 €/MWh. Finally, if waste heat is available to supply the CB, the LCOE is further reduced to 124 €/MWh, highlighting the substantial economic benefit of integrating waste-heat sources.

Figure 9 presents the DPP for the different scenarios, clearly illustrating again the strong influence of grid fees on the return period. For the complete system, the investment attractiveness is relatively low, with a DPP of

nearly 24 years. In contrast, when only the CB and ER are considered, the DPP decreases significantly to 6.2 years when grid fees are included, and further to 3.5 years when these fees are omitted. Opposite, when WH is introduced as the heat source, the ER-related revenues and grid fees disappear. Although this configuration avoids taxation, it also results in reduced overall revenue. Consequently, the DPP for the CB with waste heat becomes higher than that of the CB+ER case, despite the absence of fees. This highlights that while waste heat reduces operating costs, it also removes a source of market-driven revenue from ER operation.

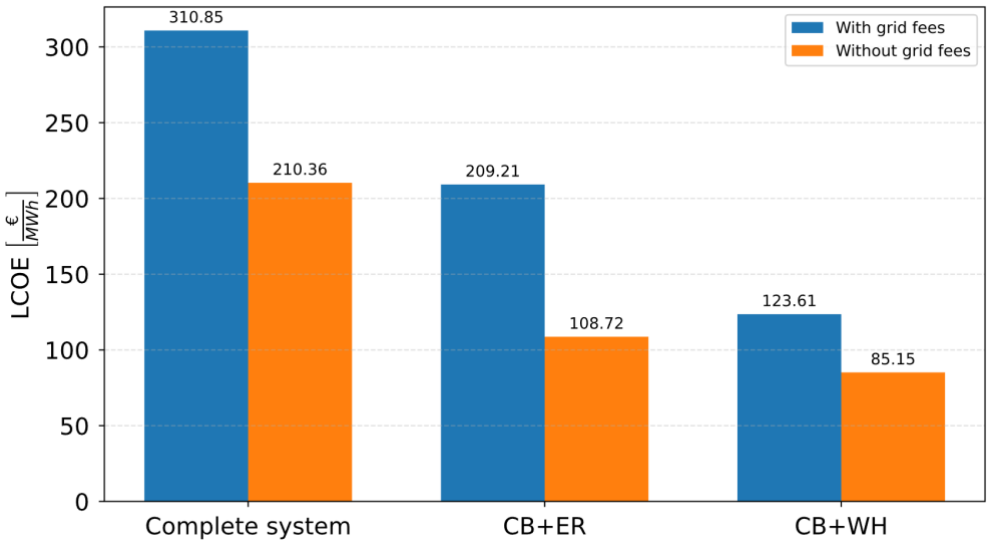

Figure 8. LCOE for the 3 different cases.

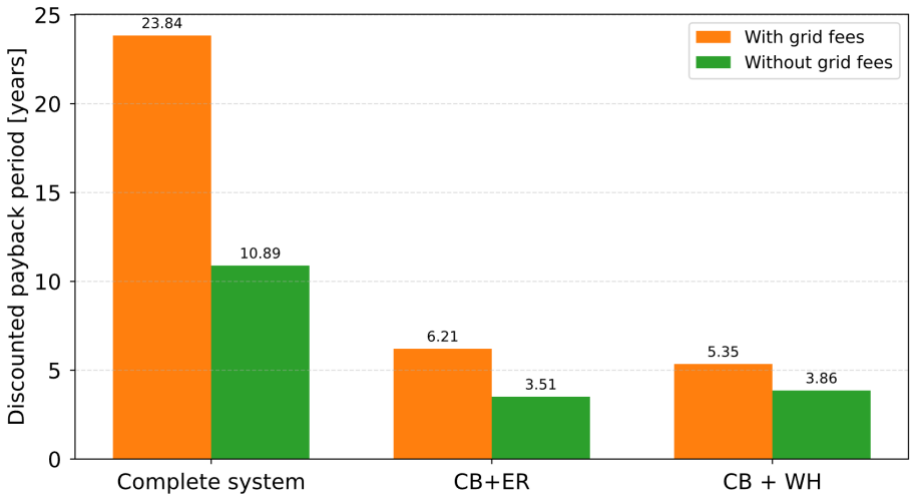

Figure 9.DPP for the 3 different cases.

7 CONCLUSIONS

This work presents and discusses the first economic assessment of integrating a reversible CB into abandoned flooded mines, demonstrating and unlocking its potential for real-world application. The analysis employs realistic economic indicators and machinery specifications, combined with extrapolated characteristics for the underground storages and the above-ground tanks. Real performance and economic data for the CB are incorporated into three comparative scenarios. The system is evaluated under 2024 market conditions using a full-year simulation with a 15-minute time step. The results highlight the significant influence of grid taxes on both the LCOE and the payback period. This emphasises the need for policymakers to support electrification strategies in coupled sectors, such as heating and electricity services, as such policies directly affect the economic viability of Carnot Battery systems. Encouragingly, the findings indicate strong potential for large-scale deployment of CBs in similar applications.

Further improvements can be achieved through system integration, such as coupling with data centers to provide cooling while reusing the resulting heat for multiple purposes, thereby reducing the system's DPP. In addition, the demonstration plant is currently under construction, and the CB is expected to be experimentally tested by mid–early 2026. These tests will provide valuable performance data for optimising the machine and validating the economic assumptions. Finally, enhanced optimisation of the control strategy has the potential to further increase revenues and/or reduce operational costs, lowering the DPP and strengthening the industrial attractiveness of CB applications.

Acknowledgements

The project that produced the results presented in this paper has received funding from the European Union's Horizon Research and Innovation programme under grant agreement No. 10112355, in the framework of the WeForming project. The authors would also like to acknowledge the funding provided by the Walloon Region of Belgium in the framework of the ARDNrgy project.

REFERENCES

Bell, I. H., Wronski, J., Quoilin, S., & Lemort, V. (2014). Pure and Pseudo-pure Fluid Thermophysical Property Evaluation and the Open-Source Thermophysical Property Library CoolProp. *Industrial & Engineering Chemistry Research*, *53*(6), 2498–2508. https://doi.org/10.1021/ie4033999

Cendoya, A., Ransy, F., Dumont, O., Guo, B., & Lemort, V. (2025). Design, Component Selection and Critical Considerations for the Development of a 50 kWe Carnot Battery Coupled to Waste Heat. In T. Turunen-Saaresti, F. Crespi, A. Spinelli, A. Uusitalo, & M. T. White (Eds.), *Proceedings of the 8th International Seminar on ORC Power Systems (ORC 2025)* (pp. 250–260). LUT Scientific and Expertise Publications. https://lutpub.lut.fi/handle/10024/170511

Cendoya, A., Ransy, F., Guo, B., Hernandez, A., Dumont, O., & Lemort, V. (2026). Design and modelling of a reversible HP/ORC Carnot battery tailored for waste heat integration in flooded mines. *Applied Energy*, *404*, 127127. https://doi.org/10.1016/j.apenergy.2025.127127

Cendoya, A., Ransy, F., Lemort, V., Dumont, O., Guo, B., & Dewallef, P. (2024, December). Numerical Modelling of a 50 kWe reversible Carnot Battery coupled with waste heat. *1st Belgian Symposium of Thermodynamics*.

Cendoya, A., Ransy, F., Lemort, V., Hernandez, A., Gresse, P.-H., & Windeshausen, J. (2024). Modelling and Simulation of a Carnot Battery Coupled to Seasonal Underground Stratified Thermal Energy Storage for Heating, Cooling and Electricity Generation. *International High Performance Buildings Conference*, 10. https://docs.lib.purdue.edu/ihpbc/472/

Elia Transmission Belgium. (2025). *Elia Open Data Portal*. https://opendata.elia.be

ENTSO-E. (2025). *ENTSO-E Transparency Platform*. https://transparency.entsoe.eu

Frate, G. F., Ferrari, L., & Desideri, U. (2020). Multi-Criteria Economic Analysis of a Pumped Thermal Electricity Storage (PTES) With Thermal Integration. *Frontiers in Energy Research*, *8*, 53. https://doi.org/10.3389/fenrg.2020.00053

Guo, B., Lemort, V., & Cendoya, A. (2025). Control Strategy and Techno-economic Optimization of a Small-scale Hybrid Energy Storage System: Reversible HP/ORC-based Carnot Battery and Electrical Battery. *Energy*, 136508. https://doi.org/10.1016/j.energy.2025.136508

Lykas, P., Bellos, E., & Tzivanidis, C. (2026). Comprehensive review and performance assessment of Carnot battery storage systems with multiple energy outputs. *Energy Conversion and Management*, *348*, 120702. https://doi.org/10.1016/j.enconman.2025.120702

Nitsch, F., Wetzel, M., Gils, H. C., & Nienhaus, K. (2024). The future role of Carnot batteries in Central Europe: Combining energy system and market perspective. *Journal of Energy Storage*, *85*, 110959. https://doi.org/10.1016/j.est.2024.110959

Pinto, M. T., Žibret, G., Lopes, L., Bodo, B., & Zajzon, N. (2020). UNEXUP: Robot-based exploration technology for underground flooded mines. *Advances in Geosciences*, *54*, 109–117. https://doi.org/10.5194/adgeo-54-109-2020

Ransy, F., Cendoya, A., & Lemort, V. (2026, July 8). *Retrofitting Abandoned Slate Mine for Long-Term Thermal Energy Storage: Lessons Learned from the WeForming and Ard-Nrgy Projects*. World Geothermal Congress 2026 (WGC2026), Calgary, Canda.